

Low-spin levels in ^{140}Sm : Five 0^+ states and the question of softness against nonaxial deformation

J. Samorajczyk-Pyśk ¹, Ch. Droste,² L. Próchniak ¹, J. Srebrny ¹, S. G. Rohoziński,² J. Andrzejewski,³ S. Dutt ⁴,
 A. Gawlik ³, K. Hadyńska-Klęk ^{1,5}, Ł. Janiak ⁶, M. Klintefjord,⁵ M. Kowalczyk ¹, J. Kowalska,¹ R. Kumar,⁷
 T. Marchlewski ¹, P. J. Napiorkowski ¹, J. Perkowski,³ W. Piątek,^{8,1} M. Piersa-Siłkowska ², T. Rogiński,² M. Saxena,^{9,10}
 A. Stolarz ¹ and A. Tucholski ¹

¹Heavy Ion Laboratory, University of Warsaw, PL 02-093 Warsaw, Poland

²Faculty of Physics, University of Warsaw, PL 02-093 Warsaw, Poland

³Faculty of Physics and Applied Computer Science, University of Łódź, PL 90-236 Łódź, Poland

⁴Department of Physics, Aligarh Muslim University, Aligarh 202002, India

⁵Department of Physics, University of Oslo, NO-0316 Oslo, Norway

⁶National Centre for Nuclear Research, Radiation Detectors and Plasma Diagnostics Division, Świerk, PL 05-400 Otwock, Poland

⁷Inter University Accelerator Centre, New Delhi 110067, India

⁸Flerov Laboratory of Nuclear Reactions, JINR, 141980 Dubna, Russia

⁹Department of Physics and Astrophysics, University of Delhi, New Delhi 110007, India

¹⁰Department of Physics and Astronomy, Ohio University, Athens, Ohio OH45701, USA



(Received 30 December 2020; accepted 21 July 2021; published 13 August 2021)

Background: Investigation of the $^{140}_{62}\text{Sm}_{78}$ nucleus, situated in the area close to the magic $N = 82$ neutron shell, offers the opportunity to find and study interesting phenomena resulting from the interplay of collective and other degrees of freedom.

Purpose: Experimental identification of low-spin low-energy levels, particularly 0^+ , in ^{140}Sm and theoretical interpretation within the collective general Bohr Hamiltonian (GBH) model.

Method: The γ - γ angular correlation technique for γ radiation after the β/EC decay of $^{140}\text{Eu} \rightarrow ^{140}\text{Sm}$ and $^{140}\text{Gd} \rightarrow ^{140}\text{Eu} \rightarrow ^{140}\text{Sm}$ was used to determine spins of excited states of ^{140}Sm . The ^{140}Gd and ^{140}Eu nuclei were produced in the $^{104}\text{Pd} + ^{40}\text{Ar}$ reaction at the HIL UW cyclotron. In the theoretical part the full five-dimensional GBH model was applied in two variants: the simple phenomenological Warsaw model and the microscopic version with six inertial functions and a potential calculated from mean-field theory.

Results: The spin and parity of six low spin (0,1,2) low lying excited levels of ^{140}Sm were measured. Two new states at around 2 MeV were identified. A analysis of the consequences of possible admixtures on the determination of the spin of a level was performed. The theoretical models applied successfully describe most of the spectrum of ^{140}Sm giving hints on the origin of the states observed in the experiment.

Conclusions: Significant softness against nonaxial deformation seems to be essential to interpret the properties of ^{140}Sm . Further experimental studies are needed to check if some low-energy excitations are not deformation driven.

DOI: [10.1103/PhysRevC.104.024322](https://doi.org/10.1103/PhysRevC.104.024322)

I. INTRODUCTION

The notion of nuclear shape plays an important role in understanding the properties of nuclei at low excitation energy. It is particularly essential for even-even nuclei, with the exception of very light ones. The shape of a nucleus, while intuitively a clear concept, cannot be easily accessed from experiment without some theoretical assumptions, especially in the case of excited states. Here, one should mention the so-called ‘sum rules’ method [1–4] which on the one hand requires a detailed knowledge of the $E2$ transitions but on the other hand gives synthetic results on the charge distribution of the ground and excited states in a model independent way. Theoretical studies have a long history starting with the concept of a deformable liquid drop or a (rotating) rigid body but recently a more realistic view of the nuclear shape is

to consider a continuous mass/charge distribution instead of a sharp surface. The distribution is usually presented in the form of a multipole expansion with the quadrupole term as the leading one. Such an approach is employed by all models using one-nucleon degrees of freedom, e.g., models based on the mean field theory.

Modern experimental techniques allow not only for extending spectroscopic studies to nuclear regions far from stability but can also provide very detailed information on the properties of stable, or close to stability, isotopes, especially on electromagnetic transitions. Often new rich data pose a real challenge for theory. Let us mention the case of the stable Cd isotopes where extensive studies [5] have led to a revision of the well-established view of these nuclei as typical examples of spherical harmonic vibrators. A similar situation can be seen in the ^{120}Te nucleus [6]. Another interesting question is

whether some of the low-energy levels in even-even nuclei can be related not to deformation-driven dynamics but to phenomena of a different nature, e.g., whether they correspond to collective excitations in the pairing sector of the mean-field (the so-called pairing vibrations [7]) or to the so-called pairing isomers [8,9]. In such cases there would be an important role for 0^+ states and information about deviations from the standard BCS picture obtained through analysis of two-nucleon transfer reactions.

In the present paper we report the results of a γ - γ correlation analysis employed to determine the spins of several levels below 3 MeV in the ^{140}Sm nucleus. The work is a continuation of extensive studies of the properties of ^{140}Sm using the Recoil Distance Doppler Shift method [10], the Coulomb excitation method [11], and the γ - γ correlation method [12]. These papers contain more detailed information on existing experimental data and theoretical results pertaining to the ^{140}Sm nucleus. Here, we briefly mention that the $^{140}\text{Sm}_{78}$ nucleus lies in the transitional region between the spherical ^{144}Sm (at the $N = 82$ shell closure) and the well-deformed isotopes around the neutron midshell. Most theoretical models predict for ^{140}Sm a rather small oblate deformation, weakly dependent on the γ variable describing triaxiality. Because of the vicinity to the neutron closed shell one would expect rather rapid changes in the properties of the Sm isotopes around $A = 140$ which creates an opportunity for finding interesting new phenomena. This requires a detailed and solid knowledge of the properties of the excited levels. Let us recall that a revision of the spin assignment of some levels [12] was crucial for the correct analysis of the Coulomb excitation data in Ref. [11].

In our experiment, the ^{140}Sm nuclei were obtained through β^+ /EC decay of the ^{140}Eu nucleus. The ground state of ^{140}Eu has spin/parity 1^+ so several low energy states with spin 0, 1, or 2 are populated in this β^+ /EC channel, which are difficult to excite using other methods. An interesting feature of the low-energy spectrum of ^{140}Sm is the existence of many (to be precise at least five) 0^+ levels. A similar phenomenon was also found in ^{134}Ba (also with $N = 78$) [13,14], using of the (p, t) transfer reaction. However, for an unstable ‘target’ nucleus two-nucleon transfer reactions are much harder to perform and for ^{140}Sm there are no data on two-neutron transfer. The origin of these 0^+ states is not quite clear—can they all be related to the shape degrees of freedom or should one look for another explanation? In an attempt to answer this question from a theoretical side, we performed calculations using two variants of the collective model: i) a simple phenomenological model with γ -independent potential energy and constant mass [15] and ii) a five-dimensional general Bohr Hamiltonian (GBH) with the potential energy and six inertial functions (mass parameters) dependent on the β, γ variables calculated in the frame of a microscopic theory [16]. The first, phenomenological, approach allows for a rather simple classification of collective levels in terms of the quantum numbers responsible for the different modes of excitation. An advantage of the second, microscopic, variant is that none of the parameters of the model is fitted to spectroscopic data.

The paper is organized as follows. In Sec. II we describe briefly the experimental method and give a detailed report on

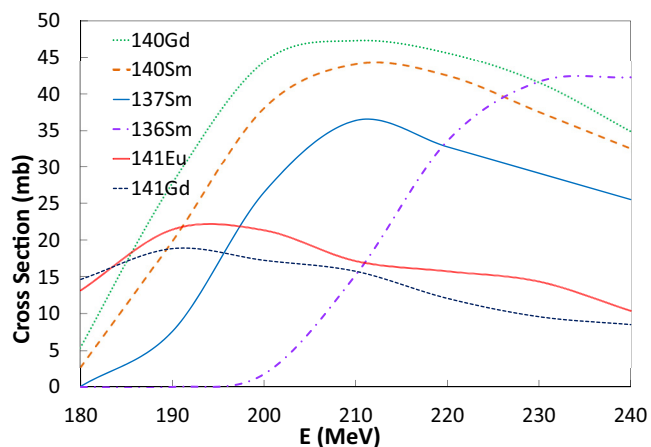


FIG. 1. Theoretical cross sections (integrated over the target and degrader thickness) for the six strongest channels for the $^{104}\text{Pd} + ^{40}\text{Ar}$ reaction.

the analysis of the data. In Sec. III we present the theoretical models and compare the results of the calculations with the experimental data. Section IV concludes the paper with a short summary of our work.

II. EXPERIMENT

A. Experimental setup

The γ - γ angular correlation method [17] was used to measure the spin values of the excited states of the ^{140}Sm nucleus. These states were populated in the β^+ /EC decay of ^{140}Gd ($T_{1/2}=15.8$ s) \rightarrow ^{140}Eu ($T_{1/2}=1.51$ s) \rightarrow ^{140}Sm ($T_{1/2}=14.8$ min) and $^{140}\text{Eu} \rightarrow ^{140}\text{Sm}$. The ^{140}Eu and ^{140}Gd nuclei were produced in the $^{104}\text{Pd} + ^{40}\text{Ar}$ reaction. An ^{40}Ar beam at 210 MeV energy was delivered by the U-200P cyclotron of the Heavy Ion Laboratory (University of Warsaw). The ion beam had a time macrostructure with 2 ms long beam-on period followed by 4 ms long beam-off period. A ^{104}Pd self-supporting target of 10 mg/cm² thickness with a Au degrader of 5 mg/cm² thickness was used. The optimal energy of the ^{40}Ar beam was determined based on the excitation function (calculated using the COMPA code [18]) and the results of a short test experiment. This code calculates cross sections (integrated over the target and degrader thickness) as functions of an ion energy. At the 210 MeV energy of the Ar ions the ^{140}Gd and ^{140}Sm nuclei are produced with a relatively high yield, as is shown in Fig. 1.

The EAGLE array [19] with 12 HPGe detectors, each one with an anti-Compton shield and a collimator, was used to register the γ rays. The relative angles between the Ge detectors were as follows: 38°, 42°, 70°, 79°, 109°, 138°, 142°, and 180° and the number of detector pairs at each angle was 4, 9, 18, 5, 18, 7, 2, and 3, respectively. The γ - γ coincidence spectra as well as singles spectra of γ quanta accompanying the ^{140}Eu and ^{140}Gd decays were registered during 4 ms off-beam periods. The singles spectra allowed the relative efficiency of Ge detectors to be determined. In this experiment about 10^8 coincidences were registered, i.e., about five times more than in our previous ^{140}Sm experiment [12].

TABLE I. Coincidences observed in the present work with gates set on the 459.9 and 531.0 keV lines (columns 3 and 4). For comparison, the results of Ref. [20] where coincidences were measured with x rays, the 459.9 and 531.0 keV lines are given (columns 5–7). In columns 1 and 2 the level energies (Refs. [20,21] and this work) and γ transition energies (Refs. [20,21]) are given.

E_{level} [keV]	E_{γ} [keV]	this work			Ref. [20]	
		coincidence with			531 keV	460 keV
		531 keV	460 keV	x rays		
530.95	531.0		+	+		+
990.64	459.9	+		+	+	
1246.52	715.4	+		+	+	
1599.1	608.6	+	+	+	+	+
	1068.0	+		+	+	
1628.65	1097.7	+		+	+	
1933.15	1402.2	+		+	+	
1951.6	1420.3	+		+		
	1952.0			+		
2022.3	1491.3	+		+	+	
2284.14	685.1				+	
	1293.6	+	+	+		
	1752.8	+		+	+	
	2283.9					
2289.88	1299.4					
	1758.7				(+)	
	2289.1					
2595.9	2064.9	+			+	

B. Data analysis and results

The γ transitions studied in the work of Firestone *et al.* (Ref. [20] and Table X therein) were ascribed to ^{140}Sm based on measurements of mass number A (determined due to mass separation), atomic number Z (due to X - γ coincidences), γ - γ coincidences, and half-life. This identification of γ rays was accepted in the present work.

In our studies, the γ - γ coincidences were measured with gates set on the $2_1^+ \rightarrow 0_1^+$; 531.0 keV and $2_2^+ \rightarrow 2_1^+$; 459.9 keV γ lines (Fig. 7). The results are presented in Table I where, for comparison, the data obtained in Ref. [20] are also given. It can be seen that most of our results is in agreement with data obtained in Ref. [20]. Some additional comments are given below.

1. The 2482.4 keV level

See Ref. [20] and Fig. 10 therein. According to Ref. [20] the 2482.4 keV state decays via emission of the 1952.0, 1491.3, and 882.7 keV γ rays. Two of the most intense cascades are as follows: γ 1952.0 keV \rightarrow γ 531.0 keV, γ 1491.3 keV \rightarrow γ 459.9 keV \rightarrow γ 531.0 keV. However, our measurement shows a lack of coincidences between the 1952.0 keV and 531.0 keV γ lines (Table I and Fig. 2). Also, the 1491.3 keV γ rays are not in coincidence with the 459.9 keV ones (Fig. 3), as they should be according to the level scheme proposed in Ref. [20]. Regarding the very weak

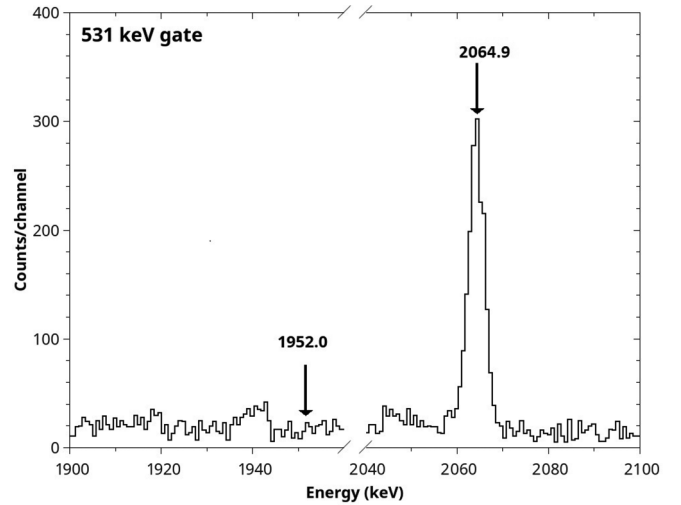


FIG. 2. Part of the γ -ray spectrum coincident with the 531.0 keV line. The expected position of the 1952.0 keV line ($I_{\gamma} = 1.4$; [20]) is marked. The 2064.9 keV line ($I_{\gamma} = 3.2$; [20]) is shown for comparison. Both intensities are normalized to $I_{\gamma}(531.0) = 100$.

882.7 keV γ line, its position in the level scheme was not uniquely determined in the present experiment. Therefore, we propose to remove this level from the scheme. It is worth noting that the 1491.3 and 1952.0 keV γ lines are used to construct two new energy levels—see Secs. II B 3 and 4.

2. The 1420.3 keV level

See Ref. [20] and Fig. 10 therein. According to Ref. [20] the level decays via emission of a 1420.3 keV γ ray directly to the ground state. However, our measurements show that this γ line is in coincidence with the 531.0 keV transition (Fig. 4). Therefore, we propose to remove this level from the scheme. The 1420.3 keV γ ray is used to construct the new level at 1951.6 keV—see Fig. 7 and Sec. II B 3.

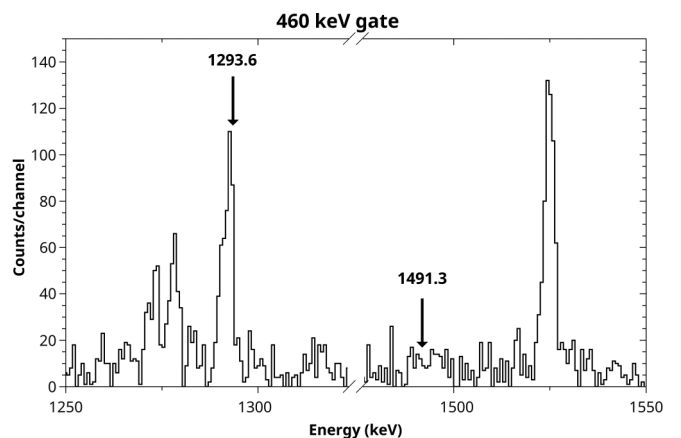


FIG. 3. Part of the γ -ray spectrum coincident with the 459.9 keV line. The expected position of the 1491.3 keV line ($I_{\gamma} = 2.1$; [20]) is marked. The 1293.6 keV line ($I_{\gamma} = 1.2$; [20]) is shown for comparison.

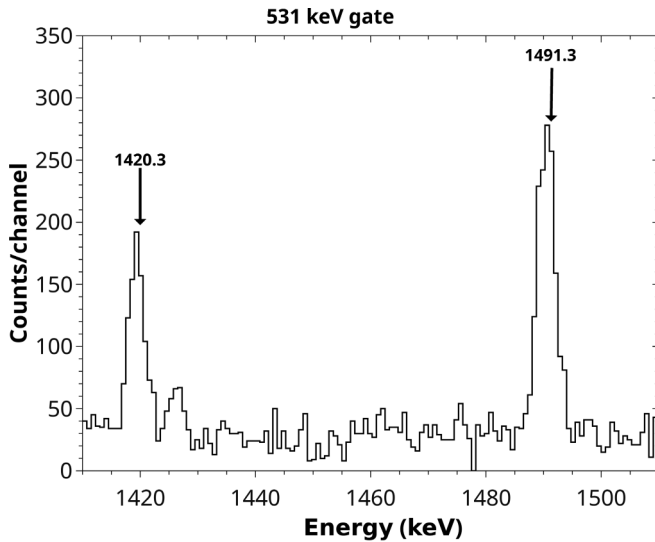


FIG. 4. Part of the γ rays spectrum (with gate set on the 531.0 keV γ line) showing that the 1420.3 keV line ($I_\gamma = 1.2$; [20]) is in coincidence with the 531.0 keV transition. The 1491.3 keV line ($I_\gamma = 2.1$; [20]) is shown for comparison.

3. The 1951.6 keV level

This is a new level proposed in the present work. This level decays via the 1420.3 and 1952.0 keV γ rays (Fig. 7). The arguments in favor of introducing such a level into the new level scheme and of removing the 1420.3 keV level proposed in Ref. [20] are as follows: according to our observation the 1420.3 keV line is in coincidence with the 531.0 keV line (Fig. 4). The 1952.0 keV transition is not in coincidence with the 531.0 keV line (Fig. 2) but belongs to the Sm nucleus, which follows from the X- γ coincidences observed in Ref. [20]. This suggests that this transition goes directly to the ground state. The energy of the 1952.0(2) keV transition fits within about two standard deviations to the sum 531.0(1)+1420.3(2) keV.

4. The 2022.3 keV level

This is a new level proposed in the present work that decays via the cascade γ 1491.3 \rightarrow γ 531.0 keV. The fact that the 1491.3 keV γ line is in coincidence with γ 531.0 keV (Table I, Fig. 4) and, moreover, is not in coincidence with γ 459.9 keV (see Fig. 3) justifies its position in the level scheme (Fig. 7). The 1491.3 keV transition is also discussed in Sec. II B 1.

5. The 2284.1 keV level

In Ref. [20] the 2284.1 keV level decays emitting the 2283.9, 1752.8, 1293.6, and 685.1 keV γ lines. The present work confirms the position of this level based on the 1293.6 and 1752.8 keV γ transitions (Table I). In the case of the 2283.9 keV line the complex singles spectrum in the vicinity of the studied line does not allow us to draw a unique conclusion about the presence of this line in the level scheme. In Ref. [20] this line is placed in the decay scheme based on energy sums. The 685.1 keV peak is not seen in our

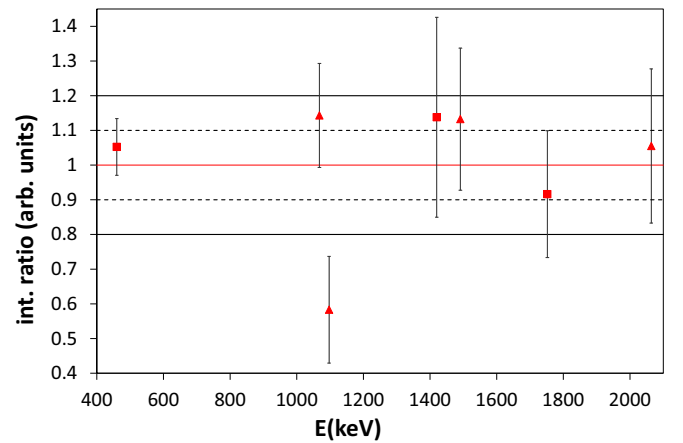


FIG. 5. The ratios of the γ transition intensities obtained in this work to the intensities given in Ref. [20]. The red symbols show the experimental intensities, the red triangles correspond to the $0 \rightarrow 2 \rightarrow 0$ cascades. The thick red line represents the weighted mean value with an error $\sigma = 12$. The four black lines deviate by $\pm 10\%$ and $\pm 20\%$ from the mean value.

spectra, therefore we can only determine the upper limit (taking into account 3σ statistical error and systematical uncertainty) $I_\gamma(685.1) \leq 0.5$. It is one-half of the value given in Ref. [20], namely 0.9(3).

The 352.4 keV γ transition (discussed in Ref. [12]) and the 882.7 keV one are not placed in the new level scheme (Fig. 7).

The intensities of the γ transitions that are the subject of the present study are compared in Fig. 5 with the results published in Ref. [20]. In our case the intensities were measured in coincidence with the $2_1^+ \rightarrow 0_1^+$; 531.0 keV γ line and corrected for the γ - γ angular correlation. Due to many radioactive chains produced in nuclear reactions on the Pd target and Au degrader the obtained singles spectrum is rather complicated and γ lines intensities cannot be determined directly from this spectrum. The intensities deviate by no more than about $\pm 15\%$ from the results of Ref. [20], except for the 1097.7 keV γ line that is discussed further.

The final results of the data analysis are summarized in Table II and Figs. 6 and 7. The results are based on the γ - γ angular correlation and $\log ft$ value analyses. The absolute intensities needed for $\log ft$ calculations were obtained by multiplying intensities normalized to $I_\gamma(531.0) = 100$ (used in Ref. [20] and in the present paper) by the factor 0.29 (see Refs. [21] and [20]). The intensities of the γ lines were taken from Ref. [20] except:

- for the 2284.1 keV level, where intensity of the 685.1 keV γ line was taken as $I_\gamma = 0.5$ (see Sec. II B 5);
- for the 1628.65 keV level, where the intensity of the 1097.7 keV γ line was taken as the average value [$I_\gamma^{\text{av}} = 1.54(27)$] based on $I_\gamma = 2.0(3)$ from Ref. [20] and $I_\gamma = 1.1(3)$ from the present work.

The intensity of the 1097 keV transition measured in our experiment differs (Fig. 5) from the value given in Ref. [20] but this difference falls within 3σ limit. This suggests that the same γ transition was observed in both experiments. For the discussed transition the experimental point ($A_{22}^{\text{exp}}, A_{44}^{\text{exp}}$) lies

TABLE II. Results of the angular correlation of γ rays in coincidence with the $2_1^+ \rightarrow 0_1^+$; 531.0 keV γ transition. Initial level and γ -transition energies ($E_{\text{level}}, E_\gamma$), the angular correlation coefficients (A_{22}, A_{44}), $\log ft$ values, spin/parity of the initial levels, and multiplicities are given. In the last column spin values known from previous work are quoted. The $\log ft$ values were calculated using the intensities of the γ lines, taken from Ref. [20] (Table X and footnote therein), except: a) for the 1628 keV level, where the intensity of the 1097 keV line was taken as the average value [$I_\gamma = 1.54(27)$] based on results of Ref. [20] and this work, see more details in Sec. II B, b) for the 2284 keV level, where intensity of the 685.1 keV γ line was taken as $I_\gamma = 0.5$ (see Sec. II B 5). To obtain the absolute intensity one should multiply the intensity normalized to $I_\gamma(531 \text{ keV}) = 100$ by the factor 0.29 (see Refs [20,21]).

E_{level}^a	E_γ^b	A_{22}	A_{44}	$\log ft$	I^π^c	Mult.	I^π previous work
1599.10	1068.0	0.37 ± 0.11	1.30 ± 0.16	5.3	0^+	$E2$	0^+ [21], $0^{(+)}$ [12]
1628.65	1097.7	0.25 ± 0.17	1.12 ± 0.25	6.1	0	$E2$ or $M2$	$0, 1, 2$ [21], (0^+) [20]
1951.6	1420.3	0.33 ± 0.16	0.02 ± 0.22	5.8	$1^{(+)}, 2^{(+)}$	$(M1 + E2)$	
2022.3	1491.3	0.49 ± 0.15	0.92 ± 0.22	5.9	$0^{(+)}$	$(E2)$	
2284.14	1752.8	-0.09 ± 0.12	-0.06 ± 0.15	5.5	$1^+, 2^+$	$M1 + E2$	2^+ [21], (2^+) [20]
2595.9	2064.9	0.34 ± 0.12	1.16 ± 0.20	5.5	0^+	$E2$	$0, 1, 2$ [21]

^aLevel energies taken from Refs. [20,21] except energies of the new levels.

^bEnergies of the γ transitions taken from Refs. [20,21].

^cIn the case of $\log ft$ about 5.9 parities are tentative. For nuclei at, or very near, closed shells the limit for allowed transitions can be smaller than 5.9 [22].

close to the $0 \rightarrow 2 \rightarrow 0$ theoretical value (Fig. 6). This means that possible admixtures have insignificant influence on the observed angular correlation, for a more detailed discussion see Appendix. Therefore, we propose spin $I_i = 0$ for the 1628.65 keV level. The parity cannot be uniquely determine since $\log ft = 6.1$.

In the case of three states (1599.1 keV, 2022.3 keV, 2595.9 keV) the measured intensities are close to those of Ref. [20] and the experimental points (A_{22}, A_{44}) of the angular correlation coefficients are grouped in the vicinity of the theoretical value for the $0 \rightarrow 2 \rightarrow 0$ cascade. This makes the assignment of the spin 0 for these levels very reliable. Low values of $\log ft$ suggest positive parities. Additional arguments for the correctness of the spin assignment are given in the Appendix.

In the case of lines 1420.3 (1951.6 keV level) and 1752.8 (2284.1 keV level) the angular correlation gives the initial spin $I_i = 1, 2, 3$, and 4 but taking into account the $\log ft$ values

(Table II) spin I_i is limited to 1 and 2. For the 2284.1 keV level we cannot find any experimental evidence to reject spin 1^+ as was done in Refs. [20] and [21].

For the 1402.2 keV line (1933.2 keV level) performing the angular correlation analysis was not possible since this line is a doublet.

Information about $E2$ transition probabilities in the ^{140}Sm nucleus is still scarce. In Table III we give known experimental [10,11] $B(E2)$ values along with theoretical predictions using models presented in the next section. From the γ -ray intensities measured in the recent experiment we estimated the

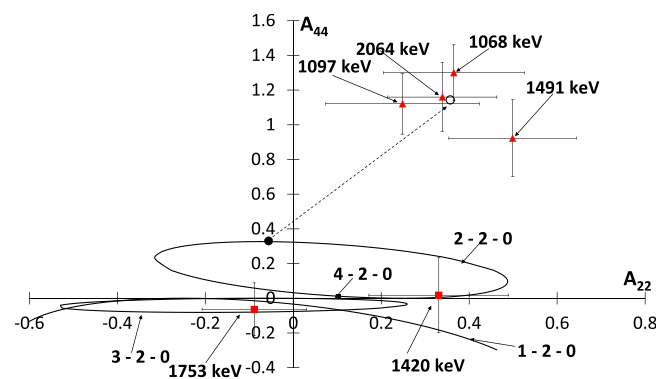


FIG. 6. Parametric plot of the A_{22} and A_{44} angular correlation coefficients. Full red symbols indicate the experimental points. The open black circle shows the theoretical (A_{22}^1, A_{44}^1) point for the $0 \rightarrow 2 \rightarrow 0$ cascade. The full black circle points to the top of the $2 \rightarrow 2 \rightarrow 0$ contour. The arrow shows a transition from the top of the $2 \rightarrow 2 \rightarrow 0$ contour to the $0 \rightarrow 2 \rightarrow 0$ one which could possibly be caused by admixtures—for more information see Appendix.

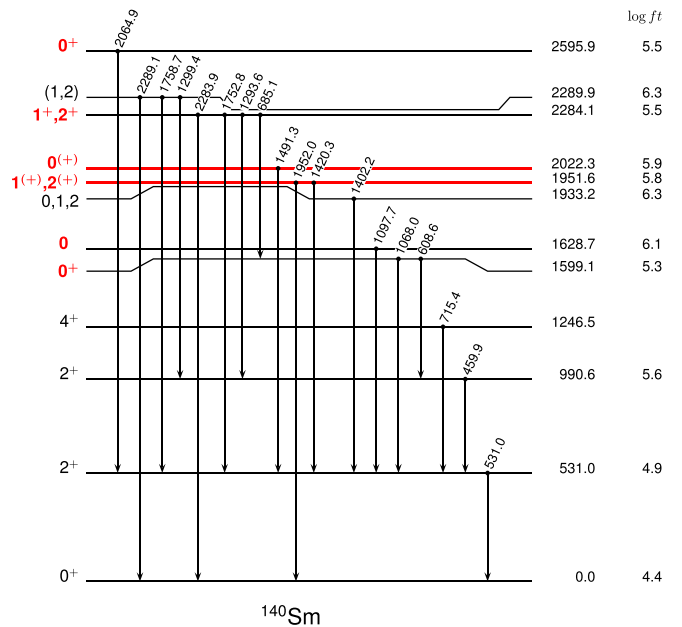


FIG. 7. Scheme of levels populated in the $^{140}\text{Eu} \rightarrow ^{140}\text{Sm}$ decay. The scheme proposed in Refs. [12,20,21] has been modified in the present work. New data are marked as solid red lines and bold digits. Spin and parity assignments are based on the γ - γ angular correlation and $\log ft$ values. For more details see text.

TABLE III. Experimental [11] and theoretical (see Sec. III) $E2$ transition probabilities in ^{140}Sm together with the spectroscopic quadrupole moment for the 2_1^+ state.

Transition	$B(E2)$ [$e^2\text{b}^2$]		
	Exp [11]	Th phen	Th micro
$2_1^+ \rightarrow 0_{\text{g.s.}}^+$	0.23 ± 0.02	0.238	0.221
$4_1^+ \rightarrow 2_1^+$	0.30 ± 0.02	0.403	0.362
$2_2^+ \rightarrow 2_1^+$	0.35 ± 0.05	0.403	0.335
$2_2^+ \rightarrow 0_{\text{g.s.}}^+$	<0.001	0.0003	0.0003
		Q_s [eb]	
2_1^+	$-0.06^{+0.41}_{-0.15}$	-0.035	-0.26

ratios of $B(E2)$ for transitions from a given excited 0^+ state to the 2_1^+ and 2_2^+ states.

A more detailed knowledge of the decay mode of the 0^+ states and, in particular, of their decay to the 2_2^+ state would be very useful in their interpretation. Unfortunately, in our experiment the $0^+ \rightarrow 2_2^+$ transition was observed only in one case and in the other three cases we were only able to establish an upper limit for the transition intensity. The estimated ratios of $B(E2)$ for transitions from a given excited 0^+ state to the 2_1^+ and 2_2^+ states are presented in Table IV.

The detailed theoretical predictions for these transitions are given in Table V in the next section. The experimental 0^+ levels are identified in Table IV by their excitation energy to make a comparison with the theory easier, because as will be seen in Sec. III, the correspondence between experimental and theoretical levels does not necessarily follow a simple ascending order of energy.

III. THEORETICAL INTERPRETATION

We present the theoretical results of two variants of the general Bohr Hamiltonian (GBH) model [16] applied to the case of ^{140}Sm . Two features of the model are worth stressing. First, all five quadrupole degrees of freedom are treated on an equal footing which makes it possible to describe all possible couplings of vibrational and rotational excitations. Second, within this model a nucleus does not have a fixed, rigid shape but is rather described by some probability distribution of various shapes. Both points are important for nuclei which are soft against deformation. In most applications of the model one uses an intrinsic (also called principal axes) reference frame where there are five variables: (β, γ) which describe

TABLE IV. Experimental estimation of ratios $B(E2, 0^+(E_x) \rightarrow 2_1^+)/B(E2, 0^+(E_x) \rightarrow 2_2^+)$ for the four lowest excited 0^+ levels (this work).

Level	$B(E2, 0^+(E_x) \rightarrow 2_1^+)/B(E2, 0^+(E_x) \rightarrow 2_2^+)$
$0^+(1599)$	0.5 ± 0.1
$0^+(1629)$	>1.4
$0^+(2022)$	>3
$0^+(2596)$	>10

TABLE V. Theoretical $B(E2)$ values for transitions from excited 0^+ states to the two lowest 2^+ states.

Transition	$B(E2)$ [$e^2\text{b}^2$]	
	Th phen	Th micro
$0_2^+ \rightarrow 2_1^+$	0.225	0.154
$0_2^+ \rightarrow 2_2^+$	0.001	0.024
$0_3^+ \rightarrow 2_1^+$	0.0006	0.016
$0_3^+ \rightarrow 2_2^+$	0.553	0.242
$0_4^+ \rightarrow 2_1^+$	0.0003	0.002
$0_4^+ \rightarrow 2_2^+$	7.3×10^{-5}	0.010
$0_5^+ \rightarrow 2_1^+$	3×10^{-6}	0.002
$0_5^+ \rightarrow 2_2^+$	0.0005	0.0002

the deformation of the nucleus and three Euler angles (Ω) giving the orientation of the intrinsic frame with respect to the laboratory frame. Over the course of the history of the model several slightly different specific definitions of the (β, γ) variables have been proposed, but generally speaking β corresponds to the elongation (or oblateness) and γ describes the triaxiality.

The most general Hamiltonian of the model (in the intrinsic frame) can be written as

$$H = T_{\text{vib}}(\beta, \gamma) + T_{\text{rot}}(\beta, \gamma, \Omega) + V(\beta, \gamma), \quad (1)$$

where

$$T_{\text{vib}} = -\frac{1}{2\sqrt{wr}} \left\{ \frac{1}{\beta^4} \left[\partial_\beta \left(\beta^4 \sqrt{\frac{r}{w}} B_{\gamma\gamma}(\beta, \gamma) \partial_\beta \right) - \partial_\beta \left(\beta^3 \sqrt{\frac{r}{w}} B_{\beta\gamma}(\beta, \gamma) \partial_\gamma \right) \right] + \frac{1}{\beta \sin 3\gamma} \left[-\partial_\gamma \left(\sqrt{\frac{r}{w}} \sin 3\gamma B_{\beta\gamma}(\beta, \gamma) \partial_\beta \right) + \frac{1}{\beta} \partial_\gamma \left(\sqrt{\frac{r}{w}} \sin 3\gamma B_{\beta\beta}(\beta, \gamma) \partial_\gamma \right) \right] \right\}, \quad (2)$$

$$T_{\text{rot}} = \frac{1}{2} \sum_{k=1}^3 \hat{I}_k^2 / J_k, \quad J_k = 4\beta^2 B_k(\beta, \gamma) \sin^2(\gamma - 2k\pi/3), \quad (3)$$

and where

$$w = B_{\beta\beta} B_{\gamma\gamma} - B_{\beta\gamma}^2, \quad r = B_1 B_2 B_3. \quad (4)$$

In Eq. (3) the operators \hat{I}_k , $k = 1, 2, 3$ are the components of the angular momentum in the intrinsic frame. The functions $B_{\beta\beta}, B_{\beta\gamma}, B_{\gamma\gamma}, B_k$ depend on the deformation variables and are called the mass parameters or, more precisely, the inertial functions, while the J_k are the moments of inertia.

Often one considers specific simpler cases of the Hamiltonian. The best known case, which can be called ‘the simplest kinetic energy’ (SKE) version, appears when all inertial functions are in fact constants and, moreover, fulfill the conditions $B = B_{\beta\beta} = B_{\gamma\gamma} = B_k$, $k = 1, 2, 3$ and $B_{\beta\gamma} = 0$. Now, the T_{vib}

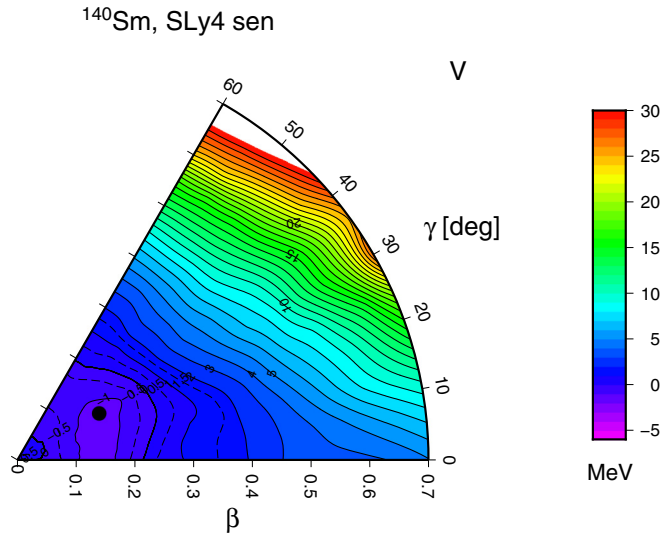


FIG. 8. Potential energy surface for ^{140}Sm calculated using the SLy4 Skyrme interaction and seniority-type pairing. Position of a minimum is marked with a black dot.

takes on the form

$$T_{\text{vib}} = -\frac{1}{2B} \left(\frac{1}{\beta^4} \partial_\beta \beta^4 \partial_\beta + \frac{1}{\beta^2 \sin 3\gamma} \partial_\gamma \sin 3\gamma \partial_\gamma \right). \quad (5)$$

In order to determine fully the Hamiltonian one needs one mass parameter B and the potential energy $V(\beta, \gamma)$, which is typically postulated as an analytic function with some free parameters. In most cases B and the parameters of the potential are somehow fitted to excited levels. A vast literature exists on this subject, see reviews [16,23,24] and references within. Such an approach we will call a phenomenological one.

Another approach consists of calculating the inertial functions and potential energy from more fundamental, microscopic mean-field theory by applying the adiabatic time dependent Hartree-Fock-Bogoliubov (ATDHFB) or the generator coordinate method (GCM) [16]. The mean field can be obtained from various nonrelativistic interactions (Skyrme, Gogny) or energy functionals as well as from relativistic mean field theory. In this case one needs to consider the most general form [Eq. (2)] of the Hamiltonian.

A. Phenomenological variant

Here, we discuss a simple phenomenological model with a γ -independent potential energy

$$V(\beta, \gamma) = V(\beta^2) = C\beta^2/2 + G[e^{-(\beta/a)^2} - 1] \quad (6)$$

and a constant mass parameter [15] (SKE). In the review [23] this model is called the ‘Warsaw solution’. The model can describe a smooth transition from the standard vibrational model to large β deformation (the Willets-Jean model [25]).

This approach offers a rather simple classification of collective excitation in terms of the quantum numbers responsible for different modes of excitation: n_β being the number of β vibrational phonons and λ describing the coupled rotational and γ -vibrational excitations (for more details see Ref. [15]).

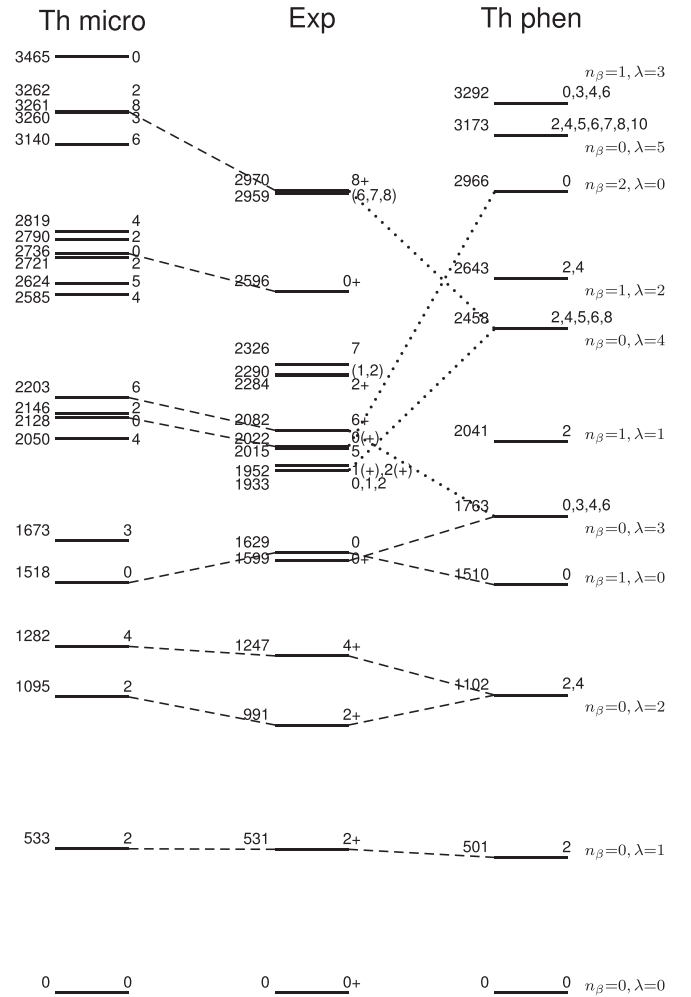


FIG. 9. Experimental and theoretical energy levels of the ^{140}Sm nucleus. The dotted lines connect levels for which a tentative correspondence is based on $B(E2)$ ratios only. For the n_β and λ labels see Sec. III A.

It also gives several useful selection rules for the $E2$ transitions. Despite being a rather crude approximation (e.g., the existence of degenerate multiplets, as can be seen in Fig. 9) it has been quite successful for transitional nuclei in the Ba region.

The calculations with the phenomenological model were performed using a potential energy with $C = 73.5$ MeV, $a = 0.103$, $G = 4.11$ MeV, and with a mass parameter $B = 135 \hbar^2/\text{MeV}$. Parameters C, a, G, B were fitted to the energy levels of ^{140}Sm . The $E2$ operator is taken as the quadrupole moment of a uniformly charged ellipsoid defined by the β, γ variables, see Eq. (15) in Ref. [15]. Hence, there is no additional parameter (effective charge) for the $E2$ transitions.

B. Microscopic variant

In the case of a microscopic variant of the GBH one does not assume a specific parametrization of the shape of the nucleus but the β, γ variables are proportional to the components of the quadrupole mass tensor (after transforming

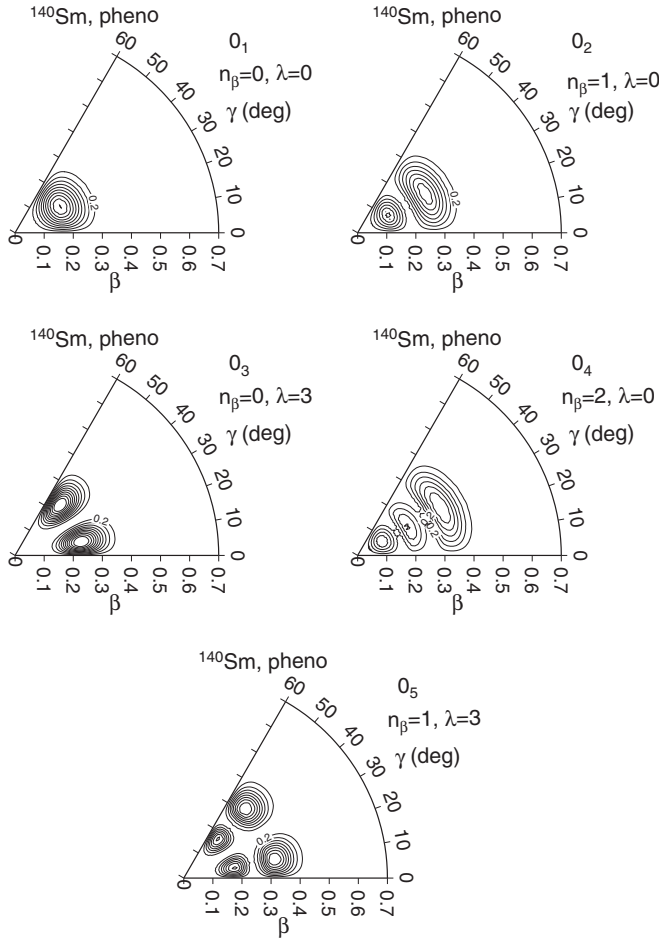


FIG. 10. Probability distributions for the five lowest 0^+ states in the phenomenological model. Distance between contour lines is 0.2 (dimensionless). One can read the n_β number from the number of knots in the radial (β) direction, while $\lambda = 0, 3$ is related with the number of knots in the angular (γ) direction.

to the intrinsic frame), for more details see, e.g., Ref. [26]. The potential energy and six inertial functions (mass parameters) which enter Eq. (2) were calculated by applying the ATDHFB method [16]. The method requires performing constrained HFB calculations of a microscopic mean-field on a grid in the β, γ plane. We used the well known SLy4 variant of the Skyrme interaction and seniority-type pairing, as in Ref. [26] with the pairing strength fixed by using odd-even mass differences so we do not have any free parameter fitted to the spectroscopic data. The $E2$ operator is also calculated microscopically and no extra effective charges are needed. We present here only a plot of the calculated potential energy in Fig. 8. The potential energy exhibits a rather weak dependence on the γ variable with a shallow minimum around $\gamma = 30^\circ$.

C. Comparison with experiment

The theoretical results of both models are compared with the experimental level scheme in Fig. 9. The phenomenological model, despite its simplicity and strong assumptions, gives a reasonable reproduction of the experimental

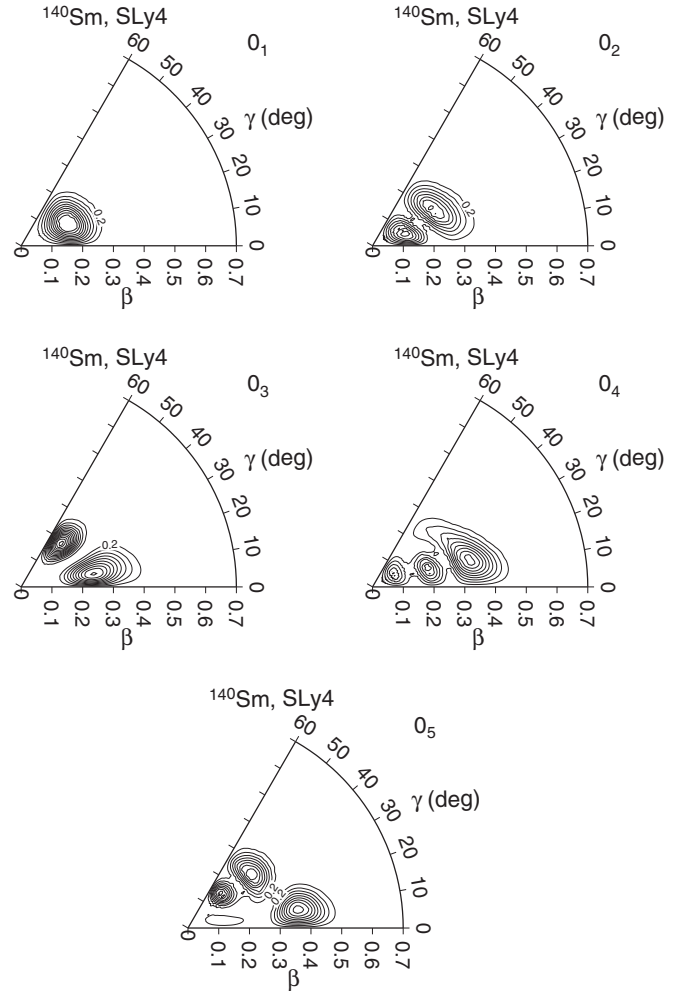


FIG. 11. Probability distributions for the five lowest 0^+ states in the microscopic model.

spectrum up to 1.5 MeV. Of particular interest are two 0^+ levels at very close energies 1599 keV and 1629 keV. Within the phenomenological model, based on the experimental $B(E2; 0 \rightarrow 2_1)/B(E2; 0 \rightarrow 2_2)$ ratio, the 1599 keV level was tentatively identified as a γ -vibrational state (with a theoretical energy equal to 1763 keV) and the 1629 keV level as a β -vibrational one (with a theoretical energy of 1510 keV). Such a nonstandard situation when the γ -vibrational 0^+ level lies very close to the β -vibrational and even a bit lower in energy is allowed by the discussed model (see Fig. 1 in Ref. [15]). Moreover, the known experimental $B(E2)$ values for decays from the $2_1^+, 2_2^+$ and 4_1^+ states (Table III) are reproduced quite well.

In the case of the microscopic model, one may note an even better agreement with experiment, e.g., energies of yrast-type levels up to spin 8 and the $I = 0$ states are reproduced with better than 10% accuracy, see Fig. 9. The theoretical $B(E2)$ transition probabilities (Table III) agree very well with experiment [11]. We stress again that in this model no parameter was fitted to spectroscopic data. A remarkable exception is the doublet of 0^+ states at around 1.6 MeV. The model predicts only one state at such an energy. The next theoretical 0 state

TABLE VI. Theoretical quadrupole invariants and the β_p, γ_p values (see text) for chosen states in ^{140}Sm , the phenomenological model.

State	$\langle Q^2 \rangle [e^2b^2]$	$\sigma(Q^2) [e^2b^2]$	$\langle Q^3 \cos 3\gamma \rangle [e^3b^3]$	$\sigma(Q^3 \cos 3\gamma) [e^3b^3]$	β_p	$\sigma(\beta_p)$	γ_p [deg]	$\sigma(\gamma_p)$ [deg]
0_1^+	1.20	0.63	0.15	1.83	0.19	0.05	28	11
0_2^+	1.78	1.19	0.37	3.68	0.23	0.08	27	11
0_3^+	1.94	0.80	0.36	3.37	0.24	0.05	28	15
0_4^+	2.38	1.69	0.69	5.87	0.27	0.10	27	11
0_5^+	2.63	1.48	0.74	5.96	0.28	0.08	27	15
2_1^+	1.42	0.68	0.20	2.24	0.21	0.05	28	11
2_2^+	1.66	0.73	0.27	2.76	0.22	0.05	28	11

lies significantly higher than the experimental one, but close to the experimental $0^{(+)}$ state at an energy of 2022 keV. This could be a hint that to explain this excitation one should consider another mechanism, e.g., related to one-particle degrees of freedom or collective pairing, possibly coupled to the deformation dynamics. However, to obtain more a conclusive answer one needs more experimental data, in particular on $E2$ transitions and spectroscopic factors from transfer reactions.

In Table III we also give data on the spectroscopic moment of the 2_1^+ state, but due to the large uncertainty in the experimental value one can say only that the theory is not in contradiction with experiment. As mentioned in the previous section, in Table V we show theoretical predictions for transitions from the excited 0^+ states discussed in this work to the $2_{1,2}^+$ states. Most theoretical $B(E2)$ are very weak and strongly depend on the details of the chosen model, so we refrain from a detailed comparison with the estimated experimental ratios of the $B(E2)$ values given in Table IV. We mention only one puzzling discrepancy between the ratio of the $B(E2)$ s from the experimental 0_4^+ level (at 2022 keV) and the calculated values of the $B(E2)$ from the theoretical (microscopic model) 0_3^+ level (Table V). The energies of these states on the other hand agree very well (Fig. 9).

Besides the energy spectra, we show in Figs. 10 and 11 the probability distributions on the β, γ plane for the five lowest 0^+ states obtained within both variants. The distributions are squares of the wave functions multiplied by the appropriate volume element, for details see, e.g., Ref. [26]. Inspection of the plots shown in Figs. 10 and 11 suggests, somewhat unexpectedly, that in the case of $0_{1,2,3,4}^+$ states the qualitative classification provided by the phenomenological model can still be useful for the more sophisticated, and hopefully more reliable, microscopic approach. These probability distributions are not accessible from experiment, but using

the sum-rule method one can evaluate the lowest moments of the distributions from the $E2$ transitions. However, this requires a very detailed knowledge of the electromagnetic transitions. In Tables VI and VII we show, for both phenomenological and microscopic models, average values of quadrupole invariants [3,4], $\langle Q^2 \rangle$ and $\langle Q^3 \cos 3\gamma \rangle$, and their dispersions: $\sigma(Q^2) = \sqrt{\langle Q^4 \rangle - \langle Q^2 \rangle^2}$ (analogous expression for $Q^3 \cos 3\gamma$) for the lowest five 0^+ and two 2^+ states. These quantities can in principle be determined from experiment. Moreover, we show in these tables the quantities β_p, γ_p which can be regarded as approximate average values of the β and γ variables, together with their dispersions, and which are calculated from the quadrupole invariants

$$\beta_p = \eta \sqrt{\langle Q^2 \rangle}, \quad (7)$$

$$\sigma(\beta_p) = \frac{\eta}{2\sqrt{\langle Q^2 \rangle}} \sqrt{\langle Q^4 \rangle - \langle Q^2 \rangle^2}, \quad (8)$$

$$\gamma_p = \frac{1}{3} \arccos \left(\frac{\langle Q^3 \cos 3\gamma \rangle}{(\langle Q^2 \rangle \langle Q^4 \rangle)^{1/2}} \right), \quad (9)$$

$$\sigma(\gamma_p) = \frac{1}{3 \sin 3\gamma_p} \sqrt{\frac{\langle (Q^3 \cos 3\gamma)^2 \rangle}{\langle Q^6 \rangle} - \frac{\langle Q^3 \cos 3\gamma \rangle^2}{\langle Q^2 \rangle \langle Q^4 \rangle}}, \quad (10)$$

where $\eta = 4\pi/3ZR^2$ with $R = r_0A^{1/3}$ and $r_0 = 1.2$ fm.

Plots of the probability distributions (Fig. 11) and quadrupole invariants (Table VII) from the microscopic theory confirm a consistent picture of the ^{140}Sm nucleus as soft against the γ deformation with an average γ close to 30° , which could be expected from the potential energy plot, Fig. 8.

A remark should be made about the probability distributions of the 0 states within the phenomenological model. As can be seen from Fig. 10 they are perfectly symmetric against the transformation $\gamma \rightarrow 60^\circ - \gamma$, which is obvious because

TABLE VII. Same as Table VI, but for the microscopic model.

State	$\langle Q^2 \rangle [e^2b^2]$	$\sigma(Q^2) [e^2b^2]$	$\langle Q^3 \cos 3\gamma \rangle [e^3b^3]$	$\sigma(Q^3 \cos 3\gamma) [e^3b^3]$	β_p	$\sigma(\beta_p)$	γ_p [deg]	$\sigma(\gamma_p)$ [deg]
0_1^+	1.12	0.55	0.27	1.58	0.18	0.05	26	11
0_2^+	1.43	1.03	0.31	2.84	0.21	0.07	27	11
0_3^+	1.95	0.99	1.09	3.64	0.24	0.06	23	15
0_4^+	2.37	1.70	2.34	5.49	0.27	0.10	20	12
0_5^+	2.77	1.78	2.25	6.76	0.29	0.09	22	15
2_1^+	1.28	0.57	0.36	1.85	0.20	0.04	26	11
2_2^+	1.44	0.59	0.23	2.14	0.21	0.04	28	10

the potential of the model does not depend on γ . Less obvious are nonzero values of mean values of the invariant ($Q^3 \cos 3\gamma$) for these states (see Table VI) and, in consequence, values of the γ_p quantity different from 30° . This is due to a term of the second order in β in the $E2$ operator, for more detailed discussion see Ref. [15].

Several theoretical predictions given in this section (Tables V, VI, and VII) cannot be compared to recently existing experimental data but we hope they are relevant for a recently performed experiment (the Coulomb excitation of ^{140}Sm at HIE-ISOLDE) or planned new ones.

IV. SUMMARY AND DISCUSSION

The ^{140}Sm nuclei were obtained from the β^+/EC decay of $^{140}\text{Eu} \rightarrow ^{140}\text{Sm}$ and $^{140}\text{Gd} \rightarrow ^{140}\text{Eu} \rightarrow ^{140}\text{Sm}$. The ^{140}Gd and ^{140}Eu nuclei were produced using beams of the Heavy Ion Laboratory (University of Warsaw) cyclotron in the $^{104}\text{Pd} + ^{40}\text{Ar}$ reaction. The experiment was performed using the EAGLE array. Our studies supplement the information from recently published results of Coulex [11] and recoil distance method (RDM) [10] measurements for ^{140}Sm . In this paper we report results for spins, parities, and multipolarities (Table II and Fig. 7) for six low-energy low-spin (0,1,2) levels of the ^{140}Sm nucleus, with a focus on the spin 0 states. This work is a continuation of our earlier study [12]. Two new levels, not reported previously in the literature, at 1951 keV and 2022 keV, respectively, have been identified. To assign the spins the γ - γ angular correlation technique was applied. Six angular correlations were measured, from which four were unambiguously identified as a result of the $0 \rightarrow 2 \rightarrow 0$ cascade. We present the details of a γ - γ angular correlation analysis and a proposed method which allowed us to estimate the influence of parasitic admixtures of unknown origin on the $0 \rightarrow 2 \rightarrow 0$ cascade (see Appendix). With this method it was proved that the identification of a $0 \rightarrow 2 \rightarrow 0$ cascade is not affected by even large (80%) admixtures. This means that the $0 \rightarrow 2 \rightarrow 0$ angular correlation is extremely ‘resistant’ to any contaminations.

To interpret the low energy spectrum of ^{140}Sm we applied two variants of the collective general Bohr Hamiltonian model: a) the simple phenomenological Warsaw model with a γ -independent potential and constant mass parameters; b) a ‘microscopic’ version where six inertial functions and the potential energy are calculated from mean-field theory. Microscopic calculations confirm a remarkable softness of the potential energy against non-axial deformation. We were interested in understanding the origin of the excited 0^+ levels, in particular of the almost degenerate 0_2 and 0_3 levels at around 1.6 MeV. The results of calculations within the phenomenological model do not exclude the possibility that this pair of levels can be related to β and γ vibrations. On the other hand the microscopic model gives a hint that one of these levels could be of a different nature, e.g., connected with pairing vibrations. It will be interesting to check these conclusions by a two-nucleon transfer reaction (with a radioactive ion beam) and more extended Coulex experiments. It is worth mentioning that one such Coulex experiment has recently been performed (University of Oslo Collaboration). Another

open question is whether the appearance of many 0^+ low-lying levels is connected with the $N = 78$ neutron number, as suggested by the results concerning ^{134}Ba in Ref. [14]. Also, for the proton number $Z = 78$ several 0 states were observed in the $^{192,194}\text{Pt}$ nuclei [27].

The microscopic version of the GBH model, with no parameters fitted to the spectroscopic data, gives a remarkably good description of the energy levels up to spin 8 and large $B(E2)$ transition probabilities for γ decay of the 2_1^+ , 2_2^+ , and 4_1^+ levels in ^{140}Sm . It appears somewhat surprising that the wave functions of the lowest levels, as well as the values of the quadrupole invariants from the microscopic variant, are very close to those obtained from the phenomenological model, which suggests that the Warsaw model could be a good first approximation to more advanced microscopic calculations.

ACKNOWLEDGMENTS

The authors wish to thank the Heavy Ion Laboratory team for providing a perfect beam. We would like also to thank Jan Kownacki and Jan Żylicz for fruitful discussions and Marek Stryczyk for a critical reading of the manuscript. This project was supported in part by Polish National Science Centre (NCN) Grant No. 2013/10/M/ST2/00427.

APPENDIX: INFLUENCE OF PARASITIC TRANSITIONS ON γ – γ ANGULAR CORRELATION RESULTS

The deviation of the measured intensity from the true value may be caused by ‘parasitic’ γ rays, i.e., γ lines being in the cascade and with energies very similar to the studied transitions. Here, we present considerations concerning the influence of possible admixtures on the result of measurements of the γ - γ angular correlations with the focus on the $0 \rightarrow 2 \rightarrow 0$ cascade.

The standard formula [12], for the γ - γ angular correlation reads

$$W_{\gamma\gamma}(\theta) = A_{00}(1 + Q_2^{\text{det.1}} Q_2^{\text{det.2}} A_{22} P_2(\cos \theta) + Q_4^{\text{det.1}} Q_4^{\text{det.2}} A_{44} P_4(\cos \theta)), \quad (\text{A1})$$

where θ denotes the angle between detectors 1 and 2, A_{00} is a cascade intensity, A_{22} and A_{44} are angular correlation coefficients, Q_2 and Q_4 are the solid angle corrections for detectors 1 and 2, and $P_2(\cos \theta)$ and $P_4(\cos \theta)$ are Legendre polynomials. The A_{kk} coefficients can be calculated from the equation quoted in Ref. [28]:

$$A_{kk} = A_k(\text{upper transition}; I_i \rightarrow I) \times A_k(\text{lower transition}; I \rightarrow I_f), \quad (\text{A2})$$

where the A_k coefficients for the upper and lower parts of the $I_i \rightarrow I \rightarrow I_f$ cascade are defined in Ref. [28]. The formula (A1) for $W_{\gamma\gamma}(\theta)$ describes the angular correlation of a ‘true’ cascade as well as a ‘parasitic’ one for appropriate values of A_{00} , A_{22} , and A_{44} . The sum of $W_{\gamma\gamma}$ functions for ‘true’ and ‘parasitic’ transitions gives the experimentally observed correlation $W_{\gamma\gamma}^{\text{eff}}$. The A_{00} , A_{22} , and A_{44} correlation coefficients for the

contaminated correlation read

$$A_{00}^{\text{eff}} = (1 + m)A_{00}^{\text{t}}$$

and, for $k = 2, 4$,

$$A_{kk}^{\text{eff}} = (A_{kk}^{\text{t}} + mA_{kk}^{\text{p}})/(1 + m), \quad (\text{A3})$$

where $m = A_{00}^{\text{p}}/A_{00}^{\text{t}}$.

The upper indices ‘eff’, ‘t’, and ‘p’ refer to effective (i.e., observed in an experiment), true, and parasitic γ - γ correlations, respectively. The study of the A_{kk} was carried out assuming multipolarity $L \leq 5$ for the upper transition and $L = 1, 2, 3$ for the lower transition (fast decays). Including the $L = 3$ component requires some additional comments. The example given below will explain. If the intermediate state decays via an electric octupole ($L = 3$) transition of an energy above 1.0 MeV (our case) then the half-life $T_{1/2}(E3)$ can be shorter than 9 ns. This quantity was calculated for the mass number $A = 150$ based on the Weisskopf estimations and the enhancement factor which for the $E3$ radiation equals 100, see Appendix 1 in Ref. [29]. The half-life for the 1 MeV $M3$ transition is longer. Hence, it is sufficient to discuss the $E3$ case only. The coincidence time of the EAGLE spectrometer is equal to 200 ns. This means that the octupole radiation (discussed above) emitted from the intermediate state of a cascade can be registered in the coincidence circuit. Hence, in the observed coincidence γ spectrum such events (also parasitic ones) will be present. This is the reason for taking the $L = 1, 2, 3$ multipolarities into account.

There is no need to calculate the A_{kk} coefficients for the $E4$, $M4$,... radiations emitted from the intermediate state since the corresponding half-lives are much longer than the coincidence time (e.g., $T_{1/2}$ for 2 MeV $E4$ radiation, $A = 150$, is equal to about $7 \mu\text{s}$). The A_{kk} coefficients for spins $I \leq 20$ were calculated according to standard formulas (cf. [30] and references therein) using our numerical program MULTIAKK.

From the whole set of A_{kk} coefficients only the largest or smallest ones were selected. Such coefficients give information about the maximum possible influence of admixtures on the results of the γ - γ angular correlations. It was found that the maximum/minimum values of A_{kk} coefficients are as follows: $A_{22,\text{max}} = 2.0$, $A_{22,\text{min}} = -1.2$, $A_{44,\text{max}} = 2.1$, $A_{44,\text{min}} = -1.6$. These extreme values occur for very low values of the intermediate spin.

A general case of the influence of admixtures on the angular correlation results is presented in Fig. 12 that shows that hypothetic ‘parasitic’ γ rays can change the value of the mixing ratio (δ) and also the spin assignment—see the left- and right-hand sides of the figure, respectively. In the particular case shown on the right side of Fig. 12 the ‘true’ initial spin $I_i = 2$ could be measured as $I_i = 1$.

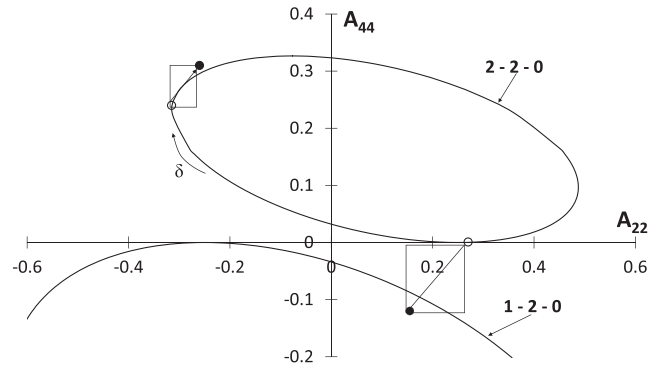


FIG. 12. The $A_{22}(\delta)$, $A_{44}(\delta)$ parametric plot for the $2 \rightarrow 2 \rightarrow 0$ and $1 \rightarrow 2 \rightarrow 0$ cascades. The ‘true’ values of (A_{22}^{t} , A_{44}^{t}) and ‘effective’ ones, i.e., the result of an admixture (A_{22}^{eff} , A_{44}^{eff}) are shown as open and full black circles, respectively. It is seen that the admixture can change the value of the mixing ratio (δ) (the left-hand side of the drawing) as well as the spin assignment (the right-hand side of the drawing). In the latter case the true spin $I_i = 2$ will be observed as $I_i = 1$.

An important conclusion comes from Eq. (A3). One can obtain the intensity of the admixtures which would cause the $2 \rightarrow 2 \rightarrow 0$ correlation to be observed as the $0 \rightarrow 2 \rightarrow 0$ case. For further analysis of ^{140}Sm the multipolarities of γ radiation emitted from the excited states of this nucleus were limited to the lowest ones, i.e., to $L = 1, 2$. The appropriate contours are presented in Fig. 6. Substituting in Eq. (A3): a) $A_{44}^{\text{t}} = 0.33$ for the top of the $2 \rightarrow 2 \rightarrow 0$ contour, b) $A_{44}^{\text{t}} = 1.14$ for the $0 \rightarrow 2 \rightarrow 0$ cascade, and c) $A_{44}^{\text{p}} = A_{44,\text{max}} = 2.1$, one gets the result that admixtures should be larger than about 80% of the $2 \rightarrow 2 \rightarrow 0$ cascade intensity. This means that only when admixtures are of such an order, the false experimental (‘effective’) points may lie in the vicinity of the theoretical (‘true’) point for the $0 \rightarrow 2 \rightarrow 0$ cascade. For a lower admixture intensity of the $2 \rightarrow 2 \rightarrow 0$ cascade the ‘effective’ point may be scattered in the (A_{22} , A_{44}) plane but does not reach the vicinity of the $0 \rightarrow 2 \rightarrow 0$ point. In the opposite case, i.e., when the $0 \rightarrow 2 \rightarrow 0$ cascade is observed as the $2 \rightarrow 2 \rightarrow 0$ one, using Eq. (A3) with $A_{44}^{\text{t}} = 1.14$, $A_{44}^{\text{eff}} = 0.33$, $A_{44}^{\text{p}} = A_{44,\text{min}} = -1.6$ leads to the conclusion that admixtures should be larger than about 40% of the $0 \rightarrow 2 \rightarrow 0$ cascade intensity. Finally, the 15% admixture cannot change the conclusion that the four experimental points, discussed above belong to the $0 \rightarrow 2 \rightarrow 0$ cascades. It follows from the discussion presented above that the $0 \rightarrow 2 \rightarrow 0$ correlations are very ‘resistant’ to any parasitic admixtures.

[1] K. Kumar, *Phys. Rev. Lett.* **28**, 249 (1972).

[2] D. Cline, *Annu. Rev. Nucl. Part. Sci.* **36**, 683 (1986).

[3] J. Srebrny, T. Czosnyka, C. Droste, S. G. Rohoziński, L. Próchniak, K. Zajac, K. Pomorski, D. Cline, C. Y. Wu, A. Backlin *et al.*, *Nucl. Phys. A* **766**, 25 (2006).

[4] J. Srebrny and D. Cline, *Int. J. Mod. Phys. E* **20**, 422 (2011).

[5] P. E. Garrett and J. L. Wood, *J. Phys. G (London)* **37**, 064028 (2010).

[6] M. Saxena, P. Napiorkowski, R. Kumar, L. Próchniak, A. Stolarz, T. Abraham, S. Dutt, M. Kicińska-Habior, M. Kisieliński, M. Komorowska *et al.*, *Acta Phys. Pol. B* **49**, 541 (2018).

- [7] D. R. Bes and R. A. Broglia, *Nucl. Phys. A* **80**, 289 (1966).
- [8] I. Ragnarsson and R. A. Broglia, *Nucl. Phys. A* **263**, 315 (1976).
- [9] J. F. Sharpey-Schafer, R. A. Bark, S. P. Bvumbi, T. R. S. Dinoko, and S. N. T. Majola, *Eur. Phys. J. A* **55**, 15 (2019).
- [10] F. L. Bello Garrote, A. Gorgen, J. Mierzejewski, C. Mihai, J. P. Delaroche, M. Girod, J. Libert, E. Sahin, J. Srebrny, T. Abraham *et al.*, *Phys. Rev. C* **92**, 024317 (2015).
- [11] M. Klintefjord, K. Hadyńska-Klęk, A. Gorgen, C. Bauer, F. L. Bello Garrote, S. Bonig, B. Bounthong, A. Damyanova, J.-P. Delaroche, V. Fedosseev *et al.*, *Phys. Rev. C* **93**, 054303 (2016).
- [12] J. Samorajczyk, M. Klintefjord, C. Droste, A. Gorgen, T. Marchlewski, J. Srebrny, T. Abraham, F. L. B. Garrote, E. Grodner, K. Hadyńska-Klęk *et al.*, *Phys. Rev. C* **92**, 044322 (2015).
- [13] G. Cata-Danil, D. Bucurescu, L. Trache, A. M. Oros, M. Jaskola, A. Gollwitzer, D. Hofer, S. Deylitz, B. D. Valnion, and G. Graw, *Phys. Rev. C* **54**, 2059 (1996).
- [14] S. Pascu, G. Cata-Danil, D. Bucurescu, N. Marginean, C. Muller, N. V. Zamfir, G. Graw, A. Gollwitzer, D. Hofer, and B. D. Valnion, *Phys. Rev. C* **81**, 014304 (2010).
- [15] S. G. Rohoziński, J. Srebrny, and K. Horbaczewska, *Z. Phys.* **268**, 401 (1974).
- [16] L. Próchniak and S. G. Rohoziński, *J. Phys. G (London)* **36**, 123101 (2009).
- [17] H. Fraunfelder and R. M. Steffen, in *Alpha- Beta- and Gamma-Ray Spectroscopy*, edited by K. Siegbahn (North-Holland, Amsterdam, 1965), Vol. 2, Chap. XIX.
- [18] J. Mierzejewski, A. A. Pasternak, M. Komorowska, J. Srebrny, E. Grodner, and M. Kowalczyk, COMPA code, <http://slcj.uw.edu.pl/pl/eagle/compa/>.
- [19] J. Mierzejewski, J. Srebrny, H. Mierzejewski, J. Andrzejewski, W. Czarnacki, C. Droste, E. Grodner, A. Jakubowski, M. Kisielinski, M. Komorowska *et al.*, *Nucl. Instrum. Methods Phys. Res. A* **659**, 84 (2011).
- [20] R. B. Firestone, J. Gilat, J. M. Nitschke, P. A. Wilmarth, and K. S. Vierinen, *Phys. Rev. C* **43**, 1066 (1991).
- [21] N. Nica, *Nucl. Data Sheets* **154**, 1 (2018).
- [22] *Nucl. Data Sheets* **124**, v (2015).
- [23] L. Fortunato, *Eur. Phys. J. A* **26**, 1 (2005).
- [24] P. Buganu and L. Fortunato, *J. Phys. G (London)* **43**, 093003 (2016).
- [25] L. Wilets and M. Jean, *Phys. Rev.* **102**, 788 (1956).
- [26] K. Wrzosek-Lipska, L. Próchniak, M. Zielińska, J. Srebrny, K. Hadyńska-Klęk, J. Iwanicki, M. Kisieliński, M. Kowalczyk, P. J. Napiorkowski, D. Pietak *et al.*, *Phys. Rev. C* **86**, 064305 (2012).
- [27] G. Ilie, R. F. Casten, P. von Brentano, D. Bucurescu, T. Faestermann, G. Graw, S. Heinze, R. Hertenberg, J. Jolie, R. Krucken *et al.*, *Phys. Rev. C* **82**, 024303 (2010).
- [28] M. Ferentz and N. Rosenzweig, in *Alpha- Beta- and Gamma-Ray Spectroscopy*, edited by K. Siegbahn (North-Holland, Amsterdam, 1965), Vol. 2, p. 1687.
- [29] *Table of Isotopes*, 8th ed., edited by R. B. Firestone and V. S. Shirley (Wiley, New York, 1996), Vol. 2.
- [30] H. W. Taylor, B. Singh, F. S. Prato, and R. McPherson, *Nucl. Data Sheets* **9**, 1 (1971).